ACS APPLIED MATERIALS & INTERFACES

www.acsami.org

Research Article

Effect of Nitro-Substituted Ending Groups on the Photovoltaic Properties of Nonfullerene Acceptors

Jing Wang,△ Yunqian Ding,△ Chenxi Li, Nan Zheng, Zengqi Xie, Zaifei Ma, Yan Lu,* Xiangjian Wan,* and Yongsheng Chen

Cite This: *ACS Appl. Mater. Interfaces* 2020, 12, 41861−41868

Read Online

ACCESS | Metrics & More | Article Recommendations | Supporting Information

ABSTRACT: Chemical modification of end groups has proved to be an effective way to design new acceptor−donor−acceptor (A−D−A)-structured nonfullerene acceptors (NFAs) for high-performance organic solar cells (OSCs). Herein, we designed and synthesized two nitro-substituted end groups, N1 and N2. Using the two end groups as A units, two A−D−A acceptors, F-N1 and F-N2, were obtained. It also has been found that the nitro substitution position on end groups affects not only the absorptions and energy levels of the resultant acceptor materials but also their molecular packing behavior and active layer morphologies. In addition, the devices based on the two acceptors showed different energy losses. Power-conversion efficiencies (PCEs) of 10.66 and 11.86% were achieved for F-N1- and F-N2-based devices, respectively. This work reveals that the nitration of end groups is one of the potential strategies for designing high-performance photovoltaic active layer materials.

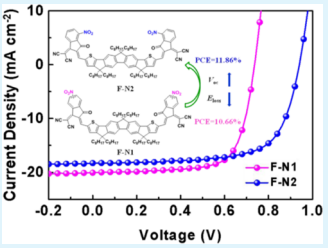

KEYWORDS: *nonfullerene acceptor, organic solar cell, nitration, ending group, power-conversion efficiency*

Downloaded via NANKAI UNIV on September 28, 2020 at 02:06:05 (UTC).
See https://pubs.acs.org/sharingguidelines for options on how to legitimately share published articles.

INTRODUCTION

Bulk-heterojunction (BHJ) organic solar cells (OSCs) have attracted extensive attention in academic and industrial areas owing to their merits of flexibility, semi-transparency, and potential of large-scale printing production.[1−8] In recent years, OSCs have made great progress and achieved power-conversion efficiencies of over 17%,[9−15] mainly thanks to the rapid development of nonfullerene acceptors (NFAs). Especially, acceptor−donor−acceptor (A−D−A)-structured NFAs have been extensively studied and demonstrated great success since the A−D−A architecture offers great convenience of fine-tuning molecular energy levels and stacking behaviors through proper choice of A and D units and/or side-chain engineering.[16−28] Over the past few years, chemical modification of end-capped groups has proved to be an effective way to design new and high-performance A−D−A-structured NFAs. Currently, the most successful end-capped group for the reported A−D−A-type NFAs is 2-(2,3-dihydro-3-oxo-1H-inden-1-ylidene) propanedinitrile (INCN) and its derivatives.[29−34] However, most of these reports were limited on halogenations by introducing halogen atoms including −F, −Cl, and −Br onto the INCN to improve the performance of the corresponding photovoltaic devices,[16,17,30,35−37] while studies of other electron-withdrawing substituents on INCN are rare to date.[38,39]

With the strong electron-withdrawing ability and unique planar structure, nitro group ($-NO_2$) has been widely used in the areas of dyes, drugs, organic semiconductor materials, etc.[40−43] Theory calculation results indicate that the D−A copolymers with nitro groups can show higher power-conversion efficiencies (PCEs) compared to −F-substituted one owing to the efficient charge transfer.[44]

In this work, two new nitrated end-capping chromophores (N1 and N2) were introduced into the A−D−A-type NFA based on the fluorenedicyclopentathiophene core to yield two new NFAs, namely, F-N1 and F-N2. It was found that the nitro substitution position on the end groups affects not only the absorptions and energy levels of the resultant F-N1 and F-N2, but also their molecular packing behavior and active layer morphologies. The photovoltaic devices based on the two acceptors fabricated with PM6 as the polymer donor exhibited PCEs of 10.66 and 11.86%, respectively. It is worthy to note that F-N1- and F-N2-based devices show comparable and promising performances in contrast to those of the devices based on their analogous molecules with the same molecular backbone (Table S1).

RESULTS AND DISCUSSION

Two nitrated end-capping chromophores (N1 and N2) were synthesized from 4-nitrophthalic anhydride and 3-nitrophthalic anhydride according to the reported procedures[23,45] (Figure 1a). The target acceptors F-N1 and F-N2 were synthesized through Knoevenagel condensation of N1 and N2 with 7,12-

Received: July 2, 2020
Accepted: August 21, 2020
Published: August 21, 2020

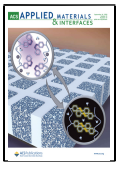

© 2020 American Chemical Society

https://dx.doi.org/10.1021/acsami.0c11698
ACS Appl. Mater. Interfaces 2020, 12, 41861−41868

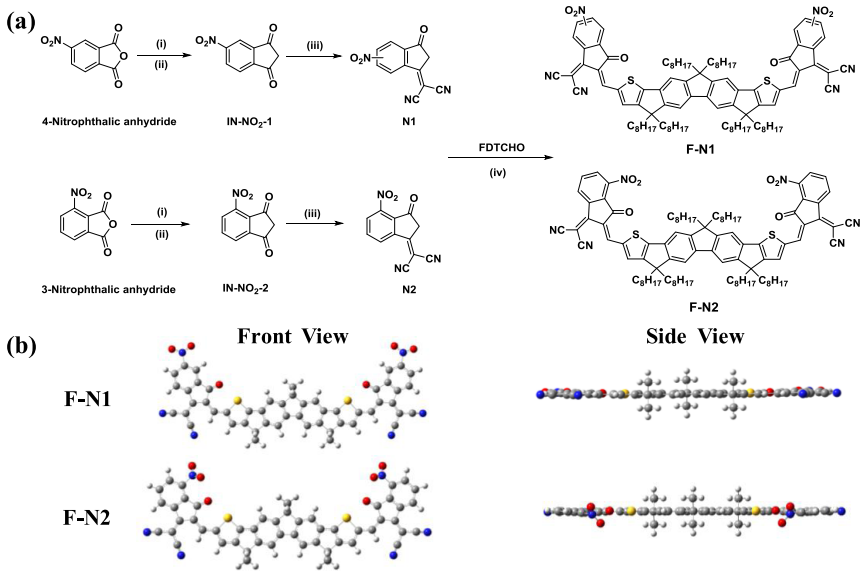

Figure 1. (a) Synthetic routes for the end groups (N1 and N2) and the two acceptors F-N1 and F-N2; (i) ethyl acetoacetate, acetic anhydride, triethylamine, CH_2Cl_2, room temperature, acidifed by HCl; (ii) trifluoroacetic acid, CH_3CN, room temperature; (iii) malononitrile, sodium acetate, CH_3CH_2OH, room temperature, acidifed by HCl; and (iv) TMSCl, DMF, $CHCl_3$, 65 °C. (b) Optimized molecular geometries of two acceptors F-N1 and F-N2 at B3LYP/6-31G(d,p) level. The octyl groups were replaced by methyl ones for simplification. Yellow atoms represent sulfur, red represents oxygen, blue represents nitrogen, and white represents hydrogen.

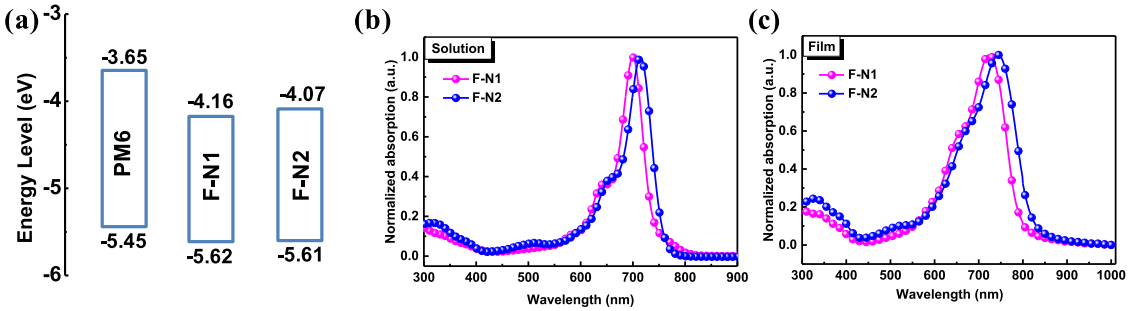

Figure 2. (a) Schematic energy-level diagrams of PM6, F-N1, and F-N2. (b) Ultraviolet−visible (UV−vis) absorption spectra of F-N1 and F-N2 in chloroform solution. (c) UV−vis absorption spectra of F-N1 and F-N2 as films.

Table 1. Measured Optical and Electrochemical Data of F-N1, F-N2, and the Reference F-H

acceptor	sol[a] λ_{max} (nm)	film[b] λ_{max} (nm)	film[b] λ_{edge} (nm)	E_g^{opt}	HOMO[c] (eV)	LUMO[c] (eV)	E_g^c CV (eV)
F-N1	714	745	830	1.49	−5.62	−4.16	1.46
F-N2	700	724	808	1.53	−5.61	−4.07	1.54
F-H	665	689	760	1.63	−5.42	−3.79	1.63

[a]Chloroform solution. [b]Thin films spin-coated from chloroform solution. [c]HOMO energy levels evaluated by CV using drop thin films; HOMO = $-(4.8 + E_{ox} - E_{Fc/Fc+})$ eV and LUMO = $-(4.8 + E_{red} - E_{Fc/Fc+})$ eV.

dihydro-4,4,7,7,12,12-hexaoctyl-4*H*-cyclopenta-[2″,1″:5,6;3″,4″:5′,6′]diindeno[1,2-b:1′,2′-b′]dithiophene-2,9-dicarbaldehyde (FDTCHO), which has a fused fluorene backbone as reported in our previous work.[22] Consequently, F-N1 is a mixture of three stereoisomers that were not separated but directly used in subsequent studies after purification. Both F-N1 and F-N2 exhibit good solubility and can be readily dissolved in various common solvents, such as chloroform, chlorobenzene, and *o*-dichlorobenzene at room temperature.

The optimal geometries of the two end groups N1 and N2 were conducted by density functional theory (DFT) simulation at the B3LYP/6-31G(d,p) level (Figure S7, SI). Although N1 is a mixture of two stereoisomers, it is found that the two oxygen atoms of the nitro group remain perfectly planar with the adjacent benzene ring and five-membered ring, while for N2, two oxygen atoms of the nitro group are not in the same planarity with the adjacent benzene ring, which should be attributed to steric hindrance between $-NO_2$ group and carbonyl group on the end-capped INCN. Further, the optimal geometries of the corresponding acceptors F-N1 and F-N2 were also conducted by a similar DFT simulation, where the octyl groups attached to fluorenedicyclopentathiophene core are replaced with methyl groups for simplification (Figure 1b). As shown in Figure 1b, the backbones of two acceptors adopt nearly planar configuration. It means that the introduction of $-NO_2$ groups to end groups does not change the primary planar configuration of the acceptor molecules.

https://dx.doi.org/10.1021/acsami.0c11698
ACS Appl. Mater. Interfaces 2020, 12, 41861−41868

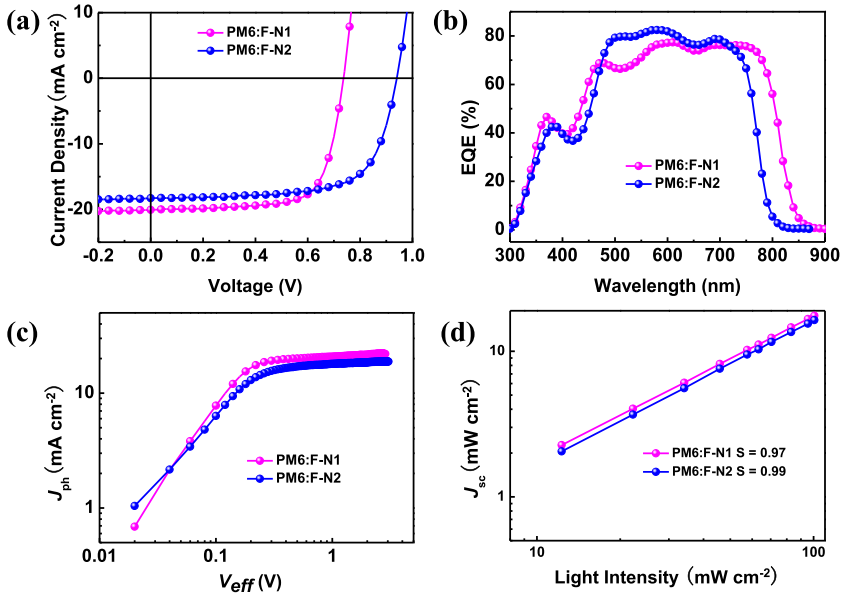

Figure 3. (a) Current density−voltage (J−V) curves for the devices based on F-N1 and F-N2 at optimized conditions under the illumination of AM 1.5G (100 mW cm^{-2}). (b) EQE curves and integrated J_{sc} for the F-N1- and F-N2-based OPV devices. (c) J_{ph} versus V_{eff} and (d) light intensity (P) dependence of J_{sc} for the optimized devices.

Table 2. Optimal Device Parameters of PM6/F-N1- and PM6/F-N2-Based Devices under the Illumination of AM 1.5G (100 mW cm^{-2})

device	V_{oc}[a] (V)	J_{sc}[a] (mA cm^{-2})	J_{cal}[b] (mA cm^{-2})	FF[a] (%)	PCE[a] (%)
PM6/F-N1	0.74 (0.73 ± 0.01)	20.06 (19.70 ± 0.57)	19.7	71.8 (70.3 ± 1.4)	10.66 (10.17 ± 0.42)
PM6/F-N2	0.94(0.94 ± 0.01)	18.28 (17.74 ± 0.27)	18.5	69.0 (68.9 ± 1.3)	11.85 (11.44 ± 0.26)

[a]All average values with standard deviations were calculated from 20 devices. [b]J_{sc} integrated from the external quantum effciency (EQE) spectrum.

However, consistent with the DFT results of N1 and N2, N1 end-capped F-N1 maintains the overall planarity extending the end of −NO_2 groups, while two oxygen atoms of nitro groups on F-N2 are not in the same planarity with the molecular backbones.

The molecular energy levels of two acceptors F-N1 and F-N2 were measured by electrochemical cyclic voltammetry (CV) (Figure S8, SI). Their energy-level diagram is presented in Figure 2a, and the corresponding highest occupied molecular orbital (HOMO), lowest unoccupied molecular orbital (LUMO), and E_g values are summarized in Table 1. The substitution position of −NO_2 groups has less impact on the HOMO levels (−5.62 eV for F-N1 and −5.61 eV for F-N2) than on the LUMO levels (−4.16 eV for F-N1 and −4.07 eV for F-N2) (Table 1). This should be attributed to the fact that LUMO levels are generally determined by the electron-withdrawing terminal units.[22] The trend in variation is in agreement with the results obtained from density functional theory (DFT) calculations (Figure S9, SI). Compared with the reference F-H without −NO_2 groups (Table 1), both HOMO and LUMO levels of F-N1 and F-N2 are down-shifted, which is similar to that of acceptors with F atom substituted INCN.[23,30]

The normalized absorption spectra of F-N1 and F-N2 in dilute chloroform solution and thin films are displayed in Figures 2b,c, and the corresponding data are also listed in Table 1. F-N1 and F-N2 exhibited maximum absorption peaks at 714 and 700 nm in the $CHCl_3$ solution and 745 and 724 nm in the film state, respectively. Compared with the absorption spectra of the two acceptors in the $CHCl_3$ solution, their absorption spectra in the film state become broader accompanied by an obvious red shift of λ_{max} over 20 nm, suggesting strong intermolecular interactions in the solid state. It was observed that the introduction of −NO_2 groups on the terminal acceptor units makes the λ_{max} of F-N1 and F-N2 red shift both in solution or in film in comparison with the counterpart without −NO_2 groups (F-H) (Table 1). From the onset of the solid absorption edge, the calculated optical band gaps (E_g^{opt}) of F-N1 and F-N2 are 1.49 and 1.53 eV, respectively, which are lower than that of F-H (1.63 eV).

OSCs devices with an inverted configuration of indium tin oxide (ITO)/ZnO/active layer/MoOx/Ag were fabricated and optimized to evaluate the photovoltaic properties using the F-N1 and F-N2 as acceptors. In view of the suitable energy levels and complementary absorption range, PM6 was selected as donor materials to blend with F-N1 and F-N2. The device parameters are summarized in Tables S2−S5. All devices were fabricated with the optimized weight ratios of PM6/F-N acceptors of 1:1. The optimized volume ratios of additive 1-chloronaphthalene (CN) for PM6/F-N1 and PM6/F-N2 were 0.8% and 1%, respectively, and thermal annealing was performed at 120 ^{o}C for 10 min. The optimal current density−voltage (J−V) curves are illustrated in Figure 3a, and the detailed device parameters are summarized in Table 2. The PM6:F-N1-based devices exhibited PCE of 10.66% with a V_{oc} of 0.74 V, a J_{sc} of 20.06 mA cm^{-2}, and an FF of 71.8%, while the PM6:F-N2-based devices achieved a higher PCE of 11.86% with a V_{oc} of 0.94 V, a J_{sc} of 18.28 mA cm^{-2}, and an FF of 69.0%. Compared with F-N2, the F-N1-based devices exhibit a higher J_{sc} mainly due to the red-shifted absorption of F-N1. In

https://dx.doi.org/10.1021/acsami.0c11698
ACS Appl. Mater. Interfaces 2020, 12, 41861−41868

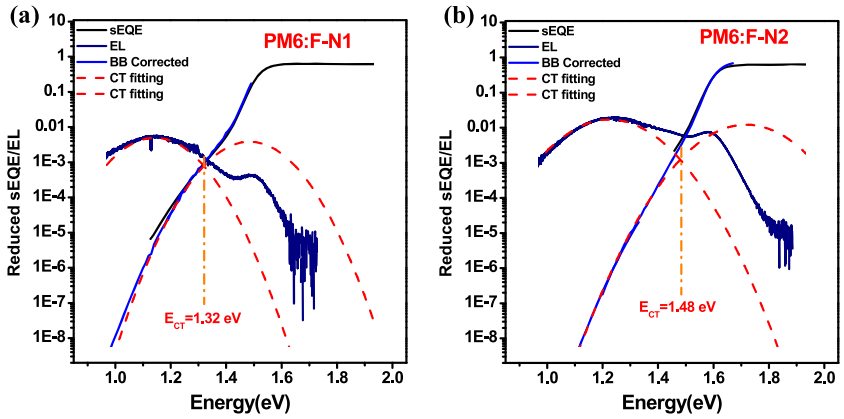

Figure 4. Reduced EL and sEQE spectra of (a) PM6:F-N1-based devices and (b) PM6:F-N2-based device with the corresponding Gaussian fitting curves for the extraction of E_{CT}. The spectral line shape of the low-energy part of the EQE spectrum is calculated from the electroluminescence spectrum, using equation EL (E)/BB (E), where BB (E) is the black body spectrum. Fittings (red dashed curve) are performed using the equation for the EQE spectrum to determine E_{CT}.[47]

Table 3. Energy Loss Analysis of PM6/F-N1- and PM6/F-N2-Based Devices

device	E_{gap} (eV)	V_{oc} (V)	E_{CT} (eV)	E_{loss} [a] (eV)	$\Delta E_1 = E_{gap} - E_{CT}$ (eV)	ΔE_2 [b] $= q\Delta V_{rad}$ (eV)	EQE_{EL}	$\Delta E_3 = q\Delta V_{non\text{-}rad}$ (eV)
PM6−F-N1	1.58	0.73	1.32	0.85	0.26	0.21	2.6×10^{-7}	0.38
PM6−F-N2	1.63	0.93	1.48	0.70	0.15	0.18	3.4×10^{-7}	0.37

[a] $E_{loss} = E_{gap} - qV_{oc}$. [b] $\Delta E_2 = E_{loss} - \Delta E_1 - \Delta E_3$.

contrast, the F-N2-based devices exhibit a higher V_{oc} owing to the lower E_{loss}, which will be discussed in detail as below.

External quantum efficiency (EQE) curves of the two acceptor-based devices are presented in Figure 3b. The F-N1-based device shows a wider photoresponse than that of the F-N2-based device. However, the EQE response of the F-N2-based device is obviously higher than that of the F-N1-based device from 470 to 630 nm, with the highest value of 82.8% at 583 nm. It may be due to the stronger absorptions of PM6:F-N2 than that of PM6:F-N1 in this region (Figure S10). The integrated photocurrents from the EQE spectra are 19.8 and 18.15 mA cm^{-2} for F-N1- and F-N2-based devices, respectively, which are consistent with the J_{sc} values obtained from $J-V$ measurements.

As shown in Figure 3c, the photocurrent (J_{ph}) versus the effective applied voltage (V_{eff}) for the two acceptor-based devices was measured. The overall charge dissociation probability under the short-circuit conditions can be estimated from the ratio of J_{ph}/J_{sat}. The J_{ph}/J_{sat} for the devices is calculated to be 92 and 97% for F-N1- and F-N2-based devices, respectively, suggesting a more efficient charge extraction for the F-N2-based devices. To investigate the relationship between charge recombination and transfer in the photoactive layer, the light intensity (P) dependence of J_{sc} was measured.[46] In Figure 3d, recombination parameters obtained by the slopes were 0.97 for PM6/F-N1-based and 0.99 for PM6:F-N2-based devices, respectively, suggesting that the bimolecular recombination for the F-N2-based device is less than that of F-N1-based device. We also studied the monomolecular recombination via treating V_{oc} as a function of P_{light}. The data were fitted to the linear law: $V_{oc} \propto \ln P_{light}$ (Figure S11, SI). The slopes for F-N1- and F-N2-based devices are 1.88 kT/q and 1.50 kT/q, respectively, indicating lower monomolecular recombination for the F-N2-based device.

The space-charge-limited current (SCLC) method was employed to measure the charge mobilities of the blend films of PM6:F-N1 and PM6:F-N2 with the electron-only and hole-only devices, respectively (Figure S12, SI). The electron and hole mobilities of the PM6:F-N1 blending film are calculated to be 1.16×10^{-4} and 2.71×10^{-4} cm^{-2} V^{-1} s^{-1}, respectively. However, the electron and hole mobilities of PM6:F-N2 blending film increase to 1.38×10^{-4} and 3.69×10^{-4} cm^{-2} V^{-1} s^{-1}, respectively. In addition, the F-N1-based film had a more balanced μ_h/μ_e ratio of 2.33 than that of the F-N2-based film with a value of 2.67. The more balanced μ_h/μ_e for PM6:F-N1 blend film is consistent with the relative higher FF.

To understand the fact that F-N2-based devices have a higher V_{oc} relative to that of the F-N1-based devices, E_{CT} and energy loss analysis of the two devices were conducted on the basis of the sensitive EQE (sEQE) and electroluminescence (EL) spectra according to the reported method.[43−45] As shown in Figure 4, the E_{CT} of F-N1 and F-N2-based devices are estimated to be 1.32 and 1.48 eV, respectively, by fitting the low-energy band in the sEQE and EL spectra, which is consistent with the fact that device based on PM6:FN-2 gave a higher V_{oc} of 0.94 V. The values of E_g^{opt} of F-N1- and F-N2-based devices are about 1.58 and 1.63 eV, respectively, which were estimated by the cross points of the normalized PL and absorption spectra of pure F-N1 and F-N2 films (Figure S13, SI). The nonradiative energy loss ($q\Delta V_{non\text{-}rad}$) is calculated by the external quantum efficiency of electroluminescence (EQE_{EL}) via the equation $q\Delta V_{non\text{-}rad} = -kT \ln(EQE_{EL})$, where q is the elementary charge, k is the Boltzmann constant, and T is the temperature.[15] The total energy loss (E_{loss}) values of F-N1- and F-N2-based devices were determined to be 0.85 and 0.70 eV, respectively, according to the formula $E_{loss} = E_g^{opt} - qV_{oc}$ (Table 3). Through disentangling the total E_{loss} into three different parts (i.e., $E_{loss} = (E_g^{opt} - E_{CT}) + (q\Delta V_{rad}) + (q\Delta V_{non\text{-}rad}) = \Delta E_1 + \Delta E_2 + \Delta E_3$),[15] it is noted that the ΔE_1, ΔE_2, and ΔE_3 based on F-N1 devices are higher than the corresponding values of F-N2-based devices. Thus, the higher

https://dx.doi.org/10.1021/acsami.0c11698
ACS Appl. Mater. Interfaces 2020, 12, 41861−41868

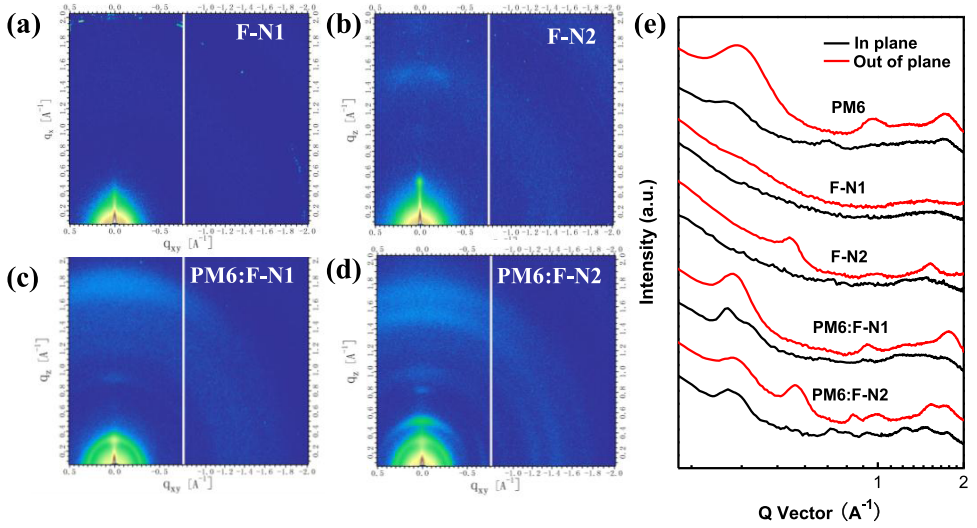

Figure 5. (a–d) Two-dimensional (2D) GIWAXS patterns for F-N1 pure film, F-N2 pure film, PM6:F-N1 blend film, and PM6:F-N2 blend film. (e) In-plane and out-of-plane line cuts of the corresponding GIWAXS patterns.

V_{oc} of the F-N2-based devices (0.94 V) compared with that of the F-N1-based devices (0.74 V) should be attributed to the higher E_{CT} and the lower E_{loss} values.

In addition, grazing incidence wide-angle X-ray scattering (GIWAXS) was employed to study the molecular packing and crystallinity[48] of the neat and blend films of F-N1 and F-N2 to further understand the effect of nitro substitution at different positions on their photovoltaic performance (Figure 5). As displayed in Figure 5a, for the F-N1 neat film, no obvious stacking peak appears whether in the out-of-plane (OOP) direction or in the in-plane (IP) direction, indicating that F-N1 does not form ordered packing in film state. While the F-N2 neat film exhibits an obvious lamellar stacking peak at 0.49 $Å^{-1}$ (d-spacing ~12.82 Å) and a distinct $\pi-\pi$ stacking peak at 1.53 $Å^{-1}$ (d-spacing ~4.11 Å) in the OOP direction (Figure 5b).

Upon blending with the polymer donor PM6, the PM6:F-N1 blend film exhibits strong scattering peaks originating from PM6 with a $\pi-\pi$ stacking peak at 1.78 $Å^{-1}$ (d-spacing ~3.52 Å) and lamellar peaks at 0.31 Å (d-spacing ~20.25 Å) in the OOP direction. In the IP direction, it presents a bimodal lamellar peak at 0.29 Å (d-spacing ~21.65 Å) and q ~0.35 Å (d-spacing ~17.94 Å), respectively (Figure 5c). Nevertheless, the PM6:F-N2 blend film shows an in-plane lamellar peak at 0.30 $Å^{-1}$ (d-spacing ~20.9 Å) and out-of-plane lamellar peak at 0.31 $Å^{-1}$ (d-spacing ~20.25 Å); the out-of-plane $\pi-\pi$ stacking peak at 1.73 $Å^{-1}$ (d-spacing ~3.63 Å) originated from the PM6 crystalline domains. The scattering peaks of F-N2 crystalline domains (out-of-plane: 0.51 and 1.51 $Å^{-1}$) can be clearly observed, indicating the maintenance of the F-N2 crystalline packing in the blend film (Figure 5d). These results indicate that more ordered packing is formed in the PM6:F-N2 blend film, which might be beneficial for the hole and electron transport.

Transmission electron microscopy (TEM) is further used to observe the morphologies of the blend films (Figure 6). As shown in Figure 6, two blend films form bicontinuous interpenetrating network, while the morphology of the blend film of PM6:F-N2 is rather homogeneous than that of blend film of PM6:F-N1. Clearly, the nitro substitution position on INCN has significant effect on the molecular packing and active layer morphologies, which might be related to the

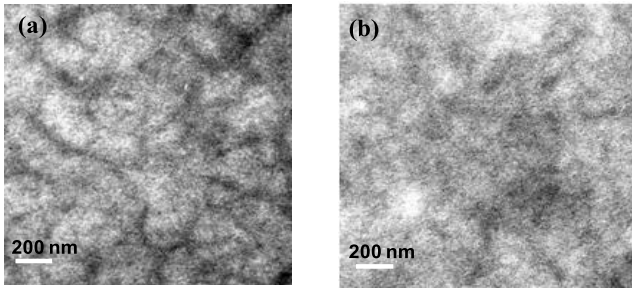

Figure 6. TEM images of (a) PM6:F-N1 blend film and (b) PM6:F-N2 blend film.

configuration of the nitro groups on INCN. These results indicate that the subtle design of nitro-substituted position on terminal groups should be considered for one strategy to design high-performance NFAs.

CONCLUSIONS

In summary, we have designed and synthesized two nitro-substituted end groups, N1 and N2. Also, two A–D–A acceptors, F-N1 and F-N2, have been synthesized employing the two end groups as the A unit. Owing to the strong electron-withdrawing ability of nitro groups, F-N1 and F-N2 showed red-shifted absorptions in contrast to the reference F-H. It also has been found that the nitro substitution position on INCN affects not only the absorptions and energy levels but also the molecular packing and the active layer morphologies. In addition, the devices based on F-N1 and F-N2 showed different E_{loss}, which can explain the difference in the V_{oc} distances between them. Although only moderate PCEs were achieved based on the two nitrated NFAs-based photovoltaic devices, it is believed that the PCEs performance can be improved by screening the other suitable donor cores and end groups of NFAs. We expect that the nitration strategy can find a wide application in developing new organic semiconductors.

EXPERIMENTAL SECTION

Materials. Chemicals were commercially purchased from commercial businesses and then used without further purification

https://dx.doi.org/10.1021/acsami.0c11698
ACS Appl. Mater. Interfaces 2020, 12, 41861–41868

unless otherwise noted. Detailed synthesis steps of N1, N2, and F-N1 and F-N2 can be found in the Supporting Information.

Device Fabrication. The photovoltaic devices were fabricated with a structure of ITO/ZnO/donor:acceptor/MoOx/Ag. The ITO-coated glass substrates were cleaned by detergent, deionized water, acetone, and isopropyl alcohol under ultrasonication for 15 min each and dried by a nitrogen blow. The sol−gel ZnO were spin-coated on the substrates and annealed at 200 °C for 1 h in the air. Then ITO substrates coated with the ZnO layer were transferred into a high-purity nitrogen-filled glovebox. The mixed PM6/F-N1 (1:1, w/w) and PM6/F-N2 (1:1, w/w) were respectively dissolved in chlorobenzene (with 0.8 vol % 1-chloronaphthalene for F-N1 and 1 vol % 1-chloronaphthalene for F-N2) to prepare 18 mg mL^{-1} blend solutions. The mixed solutions were spin-coated onto the ZnO/ITO substrates and annealed at 120 °C for 10 min to prepare the active layers. A thin molybdenum trioxide (MoOx) layer (10 nm) and a silver (Ag) layer (100 nm) were sequentially deposited by thermal evaporation.

■ ASSOCIATED CONTENT

Supporting Information

The Supporting Information is available free of charge at https://pubs.acs.org/doi/10.1021/acsami.0c11698.

Materials and synthesis; measurements and instruments; ^{1}H NMR and ^{13}C NMR spectra; high-resolution mass spectrometry; DFT calculation; CV curves; UV−vis spectra; solar cells device characterization; and device optimization (PDF)

■ AUTHOR INFORMATION

Corresponding Authors

Yan Lu − *School of Materials Science & Engineering, Tianjin Key Laboratory for Photoelectric Materials and Devices, Key Laboratory of Display Materials & Photoelectric Devices, Ministry of Education, Tianjin University of Technology, Tianjin 300384, China;* orcid.org/0000-0003-1014-7842; Email: luyan@tjut.edu.cn

Xiangjian Wan − *College of Chemistry, Nankai University, Tianjin 300071, China*; Email: xjwan@nankai.edu.cn

Authors

Jing Wang − *School of Materials Science & Engineering, Tianjin Key Laboratory for Photoelectric Materials and Devices, Key Laboratory of Display Materials & Photoelectric Devices, Ministry of Education, Tianjin University of Technology, Tianjin 300384, China*

Yunqian Ding − *College of Chemistry, Nankai University, Tianjin 300071, China*

Chenxi Li − *College of Chemistry, Nankai University, Tianjin 300071, China*

Nan Zheng − *Institute of Polymer Optoelectronic Materials and Devices, South China University of Technology, Guangzhou 510640, China*

Zengqi Xie − *Institute of Polymer Optoelectronic Materials and Devices, South China University of Technology, Guangzhou 510640, China;* orcid.org/0000-0002-9805-8176

Zaifei Ma − *Center for Advanced Low-Dimension Materials, State Key Laboratory for Modification of Chemical Fibers and Polymer Materials, Donghua University, Shanghai 201620, China;* orcid.org/0000-0002-3100-1570

Yongsheng Chen − *College of Chemistry, Nankai University, Tianjin 300071, China;* orcid.org/0000-0003-1448-8177

Complete contact information is available at: https://pubs.acs.org/10.1021/acsami.0c11698

Author Contributions

△J.W. and Y.D. contributed equally to this work.

Notes

The authors declare no competing financial interest.

■ ACKNOWLEDGMENTS

We thank Y. Gao at the Tianjin University for performing HRMS measurements. Financial support by the Natural Science Foundation of Tianjin (No. 18JCZDJC34600), the Program for Prominent Young College Teachers of Tianjin Educational Committee, and NSFC (51603149) are gratefully acknowledged.

■ REFERENCES

(1) Yu, G.; Gao, J.; Hummelen, J. C.; Wudl, F.; Heeger, A. J. Polymer Photovoltaic Cells: Enhanced Efficiencies via a Network of Internal Donor-Acceptor Heterojunctions. *Science* **1995**, *270*, 1789−1791.

(2) Chen, J.; Cao, Y. Development of Novel Conjugated Donor Polymers for High-Efficiency Bulk-Heterojunction Photovoltaic Devices. *Acc. Chem. Res.* **2009**, *42*, 1709−1718.

(3) Colsmann, A.; Puetz, A.; Bauer, A.; Hanisch, J.; Ahlswede, E.; Lemmer, U. Efficient Semi-Transparent Organic Solar Cells with Good Transparency Color Perception and Rendering Properties. *Adv. Energy Mater.* **2011**, *1*, 599−603.

(4) Patil, H.; Zu, W. X.; Gupta, A.; Chellappan, V.; Bilic, A.; Sonar, P.; Rananaware, A.; Bhosale, S. V.; Bhosale, S. V. A Non-fullerene Electron Acceptor Based on Fluorene and Diketopyrrolopyrrole Building Blocks for Solution-processable Organic Solar Cells with An Impressive Open-circuit Voltage. *Phys. Chem. Chem. Phys.* **2014**, *16*, 23837−23842.

(5) Patil, H.; Gupta, A.; Alford, B.; Ma, D.; Priver, S. H.; Bilic, A.; Sonar, P.; Bhosale, S. V. Conjoint Use of Dibenzosilole and Indan-1,3-dione Functionalities to Prepare an Efficient Non-Fullerene Acceptor for Solution-Processable Bulk-Heterojunction Solar Cells. *Asian J. Org. Chem.* **2015**, *4*, 1096−1102.

(6) Lu, L.; Zheng, T.; Wu, Q.; Schneider, A. M.; Zhao, D.; Yu, L. Recent Advances in Bulk Heterojunction Polymer Solar Cells. *Chem. Rev.* **2015**, *115*, 12666−12731.

(7) Kang, Q.; Ye, L.; Xu, B.; An, C.; Stuard, S. J.; Zhang, S.; Yao, H.; Ade, H.; Hou, J. A Printable Organic Cathode Interlayer Enables over 13% Efficiency for 1-cm(2) Organic Solar Cells. *Joule* **2019**, *3*, 227−239.

(8) Sun, Y.; Chang, M.; Meng, L.; Wan, X.; Gao, H.; Zhang, Y.; Zhao, K.; Sun, Z.; Li, C.; Liu, S.; Wang, H.; Liang, J.; Chen, Y. Flexible Organic Photovoltaics Based on Water-processed Silver Nanowire Electrodes. *Nat. Electron.* **2019**, *2*, 513−520.

(9) Luo, Z.; Ma, R.; Liu, T.; Yu, J.; Xiao, Y.; Sun, R.; Xie, G.; Yuan, J.; Chen, Y.; Chen, K.; Chai, G.; Sun, H.; Min, J.; Zhang, J.; Zou, Y.; Yang, C.; Lu, X.; Gao, F.; Yan, H. Fine-Tuning Energy Levels via Asymmetric End Groups Enables Polymer Solar Cells with Efficiencies over 17%. *Joule* **2020**, *4*, 1236−1247.

(10) Ma, R.; Liu, T.; Luo, Z.; Guo, Q.; Xiao, Y.; Chen, Y.; Li, X.; Luo, S.; Lu, X.; Zhang, M.; Li, Y.; Yan, H. Improving Open-circuit Voltage by A Chlorinated Polymer Donor Endows Binary Organic Solar Cells Efficiencies over 17%. *Sci. China Chem.* **2020**, *63*, 325−330.

(11) An, Q.; Wang, J.; Gao, W.; Ma, X.; Hu, Z.; Gao, J.; Xu, C.; Hao, M.; Zhang, X.; Yang, C.; Zhang, F. Alloy-like Ternary Polymer Solar Cells with over 17.2% Efficiency. *Sci. Bull.* **2020**, *65*, 538−545.

(12) Liu, L.; Kan, Y.; Gao, K.; Wang, J.; Zhao, M.; Chen, H.; Zhao, C.; Jiu, T.; Jen, A.-K.-Y.; Li, Y. Graphdiyne Derivative as Multifunctional Solid Additive in Binary Organic Solar Cells with 17.3% Efficiency and High Reproductivity. *Adv. Mater.* **2020**, *32*, No. 1907604.

(13) Cui, Y.; Yao, H.; Zhang, J.; Xian, K.; Zhang, T.; Hong, L.; Wang, Y.; Xu, Y.; Ma, K.; An, C.; He, C.; Wei, Z.; Gao, F.; Hou, J.

Single-Junction Organic Photovoltaic Cells with Approaching 18% Efficiency. *Adv. Mater.* **2020**, *32*, No. 1908205.
(14) Liu, Q.; Jiang, Y.; Jin, K.; Qin, J.; Xu, J.; Li, W.; Xiong, J.; Liu, J.; Xiao, Z.; Sun, K.; Yang, S.; Zhang, X.; Ding, L. 18% Efficiency organic solar cells. *Sci. Bull.* **2020**, *65*, 272−275.
(15) Luo, Z.; Ma, R.; Liu, T.; Yu, J.; Xiao, Y.; Sun, R.; Xie, G.; Yuan, J.; Chen, Y.; Chen, K.; Chai, G.; Sun, H.; Min, J.; Zhang, J.; Zou, Y.; Yang, C.; Lu, X.; Gao, F.; Yan, H. Fine-Tuning Energy Levels via Asymmetric End Groups Enables Polymer Solar Cells with Efficiencies over 17%. *Joule* **2020**, *4*, 1236−1247.
(16) Yang, F.; Li, C.; Lai, W.; Zhang, A.; Huang, H.; Li, W. Halogenated Conjugated Molecules for Ambipolar Field-effect Transistors and Non-fullerene Organic Solar Cells. *Mater. Chem. Front.* **2017**, *1*, 1389−1395.
(17) Wang, Y.; Zhang, Y.; Qiu, N.; Feng, H.; Gao, H.; Kan, B.; Ma, Y.; Li, C.; Wan, X.; Chen, Y. A Halogenation Strategy for over 12% Efficiency Nonfullerene Organic Solar Cells. *Adv. Energy Mater.* **2018**, *8*, No. 1702870.
(18) Luo, Z.; Liu, T.; Wang, Y.; Zhang, G.; Sun, R.; Chen, Z.; Zhong, C.; Wu, J.; Chen, Y.; Zhang, M.; Zou, Y.; Ma, W.; Yan, H.; Min, J.; Li, Y.; Yang, C. Reduced Energy Loss Enabled by A Chlorinated Thiophene-Fused Ending-Group Small Molecular Acceptor for Efficient Nonfullerene Organic Solar Cells with 13.6% Efficiency. *Adv. Energy Mater.* **2019**, *9*, No. 1900041.
(19) Lin, Y.; Zhang, Z.-G.; Bai, H.; Wang, J.; Yao, Y.; Li, Y.; Zhu, D.; Zhan, X. High-performance Fullerene-free Polymer Solar Cells with 6.31% Efficiency. *Energy Environ. Sci.* **2015**, *8*, 610−616.
(20) Lin, Y.; Wang, J.; Zhang, Z.-G.; Bai, H.; Li, Y.; Zhu, D.; Zhan, X. An Electron Acceptor Challenging Fullerenes for Efficient Polymer Solar Cells. *Adv. Mater.* **2015**, *27*, 1170−1174.
(21) Li, M.; Liu, Y.; Ni, W.; Liu, F.; Feng, H.; Zhang, Y.; Liu, T.; Zhang, H.; Wan, X.; Kan, B.; Zhang, Q.; Russell, T. P.; Chen, Y. A Simple Small Molecule as An Acceptor for Fullerene-free Organic Solar Cells with Efficiency Near 8%. *J. Mater. Chem. A* **2016**, *4*, 10409−10413.
(22) Qiu, N.; Zhang, H.; Wan, X.; Li, C.; Ke, X.; Feng, H.; Kan, B.; Zhang, H.; Zhang, Q.; Lu, Y.; Chen, Y. A New Nonfullerene Electron Acceptor with a Ladder Type Backbone for High-Performance Organic Solar Cells. *Adv. Mater.* **2017**, *29*, No. 1604964.
(23) Dai, S.; Zhao, F.; Zhang, Q.; Lau, T.-K.; Li, T.; Liu, K.; Ling, Q.; Wang, C.; Lu, X.; You, W.; Zhan, X. Fused Nonacyclic Electron Acceptors for Efficient Polymer Solar Cells. *J. Am. Chem. Soc.* **2017**, *139*, 1336−1343.
(24) Yuan, J.; Zhang, Y.; Zhou, L.; Zhang, G.; Yip, H.-L.; Lau, T.-K.; Lu, X.; Zhu, C.; Peng, H.; Johnson, P. A.; Leclerc, M.; Cao, Y.; Ulanski, J.; Li, Y.; Zou, Y. Single-Junction Organic Solar Cell with over 15% Efficiency Using Fused-Ring Acceptor with Electron-Deficient Core. *Joule* **2019**, *3*, 1140−1151.
(25) Zhou, Z.; Liu, W.; Zhou, G.; Zhang, M.; Qian, D.; Zhang, J.; Chen, S.; Xu, S.; Yang, C.; Gao, F.; Zhu, H.; Liu, F.; Zhu, X. Subtle Molecular Tailoring Induces Significant Morphology Optimization Enabling over 16% Efficiency Organic Solar Cells with Efficient Charge Generation. *Adv. Mater.* **2020**, *32*, No. 1906324.
(26) Lin, Y.; Zhao, F.; He, Q.; Huo, L.; Wu, Y.; Parker, T. C.; Ma, W.; Sun, Y.; Wang, C.; Zhu, D.; Heeger, A. J.; Marder, S. R.; Zhan, X. High-Performance Electron Acceptor with Thienyl Side Chains for Organic Photovoltaics. *J. Am. Chem. Soc.* **2016**, *138*, 4955−4961.
(27) Yang, Y.; Zhang, Z.-G.; Bin, H.; Chen, S.; Gao, L.; Xue, L.; Yang, C.; Li, Y. Side-Chain Isomerization on An n-type Organic Semiconductor ITIC Acceptor Makes 11.77% High Efficiency Polymer Solar Cells. *J. Am. Chem. Soc.* **2016**, *138*, 15011−15018.
(28) Jiang, K.; Wei, Q.; Lai, J. Y. L.; Peng, Z.; Kim, H. K.; Yuan, J.; Ye, L.; Ade, H.; Zou, Y.; Yan, H. Alkyl Chain Tuning of Small Molecule Acceptors for Efficient Organic Solar Cells. *Joule* **2019**, *3*, 3020−3033.
(29) Liu, X.; Wang, X.; Xiao, Y.; Yang, Q.; Guo, X.; Li, C. H-Bonds-Assisted Molecular Order Manipulation of Nonfullerene Acceptors for Efficient Nonannealed Organic Solar Cells. *Adv. Energy Mater.* **2020**, *10*, No. 1903650.
(30) Kim, I.-B.; Jang, S.-Y.; Kim, Y.-A.; Kang, R.; Kim, I.-S.; Ko, D.-K.; Kim, D.-Y. The Effect of Fluorine Substitution on the Molecular Interactions and Performance in Polymer Solar Cells. *ACS Appl. Mater. Interfaces* **2017**, *9*, 24011−24019.
(31) Li, S.; Ye, L.; Zhao, W.; Zhang, S.; Ade, H.; Hou, J. Significant Influence of the Methoxyl Substitution Position on Optoelectronic Properties and Molecular Packing of Small-Molecule Electron Acceptors for Photovoltaic Cells. *Adv. Energy Mater.* **2017**, *7*, No. 1700183.
(32) Feng, H.; Qiu, N.; Wang, X.; Wang, Y.; Kan, B.; Wan, X.; Zhang, M.; Xia, A.; Li, C.; Liu, F.; Zhang, H.; Chen, Y. An A-D-A Type Small-Molecule Electron Acceptor with End-Extended Conjugation for High Performance Organic Solar Cells. *Chem. Mater.* **2017**, *29*, 7908−7917.
(33) Yao, H.; Ye, L.; Hou, J.; Jang, B.; Han, G.; Cui, Y.; Su, G. M.; Wang, C.; Gao, B.; Yu, R.; Zhang, H.; Yi, Y.; Woo, H. Y.; Ade, H.; Hou, J. Achieving Highly Efficient Nonfullerene Organic Solar Cells with Improved Intermolecular Interaction and Open-Circuit Voltage. *Adv. Mater.* **2017**, *29*, No. 1700254.
(34) Luo, Z.; Bin, H.; Liu, T.; Zhang, Z.-G.; Yang, Y.; Zhong, C.; Qiu, B.; Li, G.; Gao, W.; Xie, D.; Wu, K.; Sun, Y.; Liu, F.; Li, Y.; Yang, C. Fine-Tuning of Molecular Packing and Energy Level through Methyl Substitution Enabling Excellent Small Molecule Acceptors for Nonfullerene Polymer Solar Cells with Efficiency up to 12.54%. *Adv. Mater.* **2018**, *30*, No. 1706124.
(35) Cui, Y.; Yao, H.; Zhang, J.; Zhang, T.; Wang, Y.; Hong, L.; Xian, K.; Xu, B.; Zhang, S.; Peng, J.; Wei, Z.; Gao, F.; Hou, J. Over 16% Efficiency Organic Photovoltaic Cells Enabled by A Chlorinated Acceptor with Increased Open-circuit Voltages. *Nat. Commun.* **2019**, *10*, No. 2515.
(36) Sun, C.; Qin, S.; Wang, R.; Chen, S.; Pan, F.; Qiu, B.; Shang, Z.; Meng, L.; Zhang, C.; Xiao, M.; Yang, C.; Li, Y. High Efficiency Polymer Solar Cells with Efficient Hole Transfer at Zero Highest Occupied Molecular Orbital Offset between Methylated Polymer Donor and Brominated Acceptor. *J. Am. Chem. Soc.* **2020**, *142*, 1465−1474.
(37) Zhao, W.; Li, S.; Yao, H.; Zhang, S.; Zhang, Y.; Yang, B.; Hou, J. Molecular Optimization Enables over 13% Efficiency in Organic Solar Cells. *J. Am. Chem. Soc.* **2017**, *139*, 7148−7151.
(38) Lai, H.; Zhao, Q.; Chen, Z.; Chen, H.; Chao, P.; Zhu, Y.; Lang, Y.; Zhen, N.; Mo, D.; Zhang, Y.; He, F. Trifluoromethylation Enables a 3D Interpenetrated Low-Band-Gap Acceptor for Efficient Organic Solar Cells. *Joule* **2020**, *4*, 688−700.
(39) Yao, C.; Zhao, J.; Zhu, Y.; Liu, B.; Yan, C.; Perepichka, D. F.; Meng, H. Trifluoromethyl Group-Modified Non-Fullerene Acceptor toward Improved Power Conversion Efficiency over 13% in Polymer Solar Cells. *ACS Appl. Mater. Interfaces* **2020**, *12*, 11543−11550.
(40) Hartmann, H.; Eckert, K.; Schroder, A. New Solvatochromic Dyes of the 5-dimethyl-amino-5′ nitro-2,2′-bithiophene Type. *Angew. Chem., Int. Ed.* **2000**, *39*, 556−558.
(41) Nepali, K.; Lee, H.-Y.; Liou, J.-P. Nitro-Group-Containing Drugs. *J. Med. Chem.* **2019**, *62*, 2851−2893.
(42) de Melo, C. E. A.; Nandi, L. G.; Domínguez, M.; Rezende, M. C.; Machado, V. G. Solvatochromic Behavior of Dyes with Dimethylamino Electron-donor and Nitro Electron-acceptor Groups in Their Molecular Structure. *J. Phys. Org. Chem.* **2015**, *28*, 250−260.
(43) Srivani, D.; Gupta, A.; Raynor, A. M.; Bilic, A.; Li, J.; Bhosale, S. V.; Bhosale, S. V. Naphthalene Diimide-based Non-fullerene Acceptors for Simple, Efficient, and Solution-processable Bulk-heterojunction Devices. *RSC Adv.* **2016**, *6*, 38703−38708.
(44) Zamora, P. P.; Bieger, K.; Vasquez, D.; Merino, M.; Maurelia, R. Effect of Nitro Groups on Electrochemical and Photovoltaic Behavior of Tris-thiophenes used in Organic Solar Cells. *Int. J. Electrochem. Sci.* **2015**, *10*, 10321−10335.
(45) Rajur, R.; Rao, V. N.; Kim, H.-O.; Nagafuji, P.; Hearult, X.; Williams, J. D.; Peet, N. P. Efficient Synthesis of 7-Amino-3-hydroxyindan-1-one. *Synth. Commun.* **2009**, *39*, 626−635.
(46) Riedel, I.; Parisi, J.; Dyakonov, V.; Lutsen, L.; Vanderzande, D.; Hummelen, J. C. Effect of Temperature and Illumination on the

https://dx.doi.org/10.1021/acsami.0c11698
ACS Appl. Mater. Interfaces 2020, 12, 41861−41868

Electrical Characteristics of Polymer-fullerene Bulk-heterojunction Solar Cells. *Adv. Funct. Mater.* **2004**, *14*, 38−44.
(47) Tang, Z.; Wang, J.; Melianas, A.; Wu, Y.; Kroon, R.; Li, W.; Ma, W.; Andersson, M. R.; Ma, Z.; Cai, W.; Tress, W.; Inganas, O. Relating open-circuit voltage losses to the active layer morphology and contact selectivity in organic solar cells. *J. Mater. Chem. A* **2018**, *6*, 12574−12581.
(48) Müller-Buschbaum, P. The Active Layer Morphology of Organic Solar Cells Probed with Grazing Incidence Scattering Techniques. *Adv. Mater.* **2014**, *26*, 7692−7709.

https://dx.doi.org/10.1021/acsami.0c11698
ACS Appl. Mater. Interfaces 2020, 12, 41861−41868